Controlling Nanocrystal Density and Location on Carbon Nanotube Templates

Xiaohui Peng[†] and Stanislaus S. Wong[†,‡,*]

Department of Chemistry, State University of New York at Stony Brook, Stony Brook, New York 11794-3400, and Materials and Chemical Sciences Department, Brookhaven National Laboratory, Building 480, Upton, New York 11973

Received September 29, 2008. Revised Manuscript Received November 28, 2008

We have demonstrated a covalent route toward site-selective synthesis of MWNT−nanoparticle conjugates containing two different types of nanoscale species, i.e., Au nanoparticles and CdSe QDs. We have quantitatively probed the effects of varying oxidation treatments, precursor concentrations, and incubation times in order to rationally affect the spatial coverage and distribution of either Au NPs or semiconducting QDs on the MWNT sidewalls and tips. The degree of nanoparticulate coverage was found to primarily vary with the intensity of the oxidation treatment, though the hydrophobicity of the nanotube as well as the chemical and steric characteristics of the nanocrystals also played a role in determining the ultimate architecture. In general, the stronger the oxidation treatment, the denser the coating of nanoparticles and/or quantum dots on the nanotube surface. In addition, the use of larger concentrations of precursor nanocrystals along with longer incubation times was conducive to the observation of higher nanoparticle densities on our nanotube templates. Interesting charge transfer, electromagnetic enhancement, and energy-transfer behavior between CNTs and the corresponding nanoparticles/quantum dots have been observed and will likely render such conjugates as key components in a range of nanoscale devices important for photocatalytic and solar applications.

1. Introduction to Nanotube−Nanocrystal Heterostructures

Over the years, we and many other groups have expended a lot of effort in creating discrete assemblies composed of nanoparticle/nanocrystal motifs attached to carbon nanotubes (CNTs).[1−4] A key scientific issue associated with this model system is whether such nanomaterial heterostructures can provide for efficient pathways for charge separation relative to loss mechanisms such as recombination. It is not surprising therefore that carbon nanotube−nanocrystal heterostructures have been intensively studied for their potential incorporation into nanoscale devices, such as light harvesting photovoltaic cells,[5–8] chemical sensors,[9–11] fluorescent nanoprobes,[12,13] and heterogeneous catalysts.[14,15]

Several strategies have already been put forward for the fabrication of CNT−nanoparticle heterostructures. Generally, either nanoparticles or quantum dots (QDs) can be attached to either the tips or defect sites along the sidewalls of CNTs via either covalent[1,2,16] (through the formation of discrete bonds) or noncovalent (e.g., through wrapping and/or manipulation of relatively nonspecific hydrophobic interactions) strategies.[3,17–21] Moreover, other protocols for preparing nanotube-nanocrystal conjugates have been associated with

* To whom correspondence should be addressed. Phone: (631) 632-1703; (631) 344-3178. E-mail:sswong@notes.cc.sunysb.edu; sswong@bnl.gov.
† State University of New York at Stony Brook.
‡ Brookhaven National Laboratory.

(1) Banerjee, S.; Wong, S. S. *Nano Lett.* **2002**, *2* (3), 195–200.
(2) Azamian, B. R.; Coleman, K. S.; Davis, J. J.; Hanson, N.; Green, M. L. H. *Chem. Commun.* **2002**, 366–367.
(3) Ellis, A. V.; Vijayamohanan, K.; Goswami, R.; Chakrapani, N.; Ramanathan, L. S.; Ajayan, P. M.; Ramanath, G. *Nano Lett.* **2003**, *3* (3), 279–282.
(4) Choi, H. C.; Shim, M.; Bangsaruntip, S.; Dai, H. J. *J. Am. Chem. Soc.* **2002**, *124* (31), 9058–9059.
(5) Sheeney-Haj-Khia, L.; Basnar, B.; Willner, I. *Angew. Chem., Int. Ed.* **2005**, *44* (1), 78–83.
(6) Cho, N.; Choudhury, K. R.; Thapa, R. B.; Sahoo, Y.; Ohulchanskyy, T.; Cartwright, A. N.; Lee, K. S.; Prasad, P. N. *Adv. Mater.* **2007**, *19* (2), 232–236.
(7) Guldi, D. M.; Rahman, G. M. A.; Sgobba, V.; Kotov, N. A.; Bonifazi, D.; Prato, M. *J. Am. Chem. Soc.* **2006**, *128* (7), 2315–2323.
(8) Kongkanand, A.; Dominguez, R. M.; Kamat, P. V. *Nano Lett.* **2007**, *7* (3), 676–680.
(9) Mubeen, S.; Zhang, T.; Yoo, B.; Deshusses, M. A.; Myung, N. V. *J. Phys. Chem. C* **2007**, *111* (17), 6321–6327.
(10) Star, A.; Joshi, V.; Skarupo, S.; Thomas, D.; Gabriel, J. C. P. *J. Phys. Chem. B* **2006**, *110* (42), 21014–21020.
(11) Kang, X. H.; Mai, Z. B.; Zou, X. Y.; Cai, P. X.; Mo, J. Y. *J. Nanosci. Nanotechnol.* **2007**, *7* (4−5), 1618–1624.
(12) Bottini, M.; Cerignoli, F.; Dawson, M. I.; Magrini, A.; Rosato, N.; Mustelin, T. *Biomacromolecules* **2006**, *7* (8), 2259–2263.
(13) Jia, N. Q.; Lian, Q.; Shen, H. B.; Wang, C.; Li, X. Y.; Yang, Z. N. *Nano Lett.* **2007**, *7* (10), 2976–2980.
(14) Han, L.; Wu, W.; Kirk, F. L.; Luo, J.; Maye, M. M.; Kariuki, N. N.; Lin, Y. H.; Wang, C. M.; Zhong, C. J. *Langmuir* **2004**, *20* (14), 6019–6025.
(15) Pan, X. L.; Fan, Z. L.; Chen, W.; Ding, Y. J.; Luo, H. Y.; Bao, X. H. *Nat. Mater.* **2007**, *6* (7), 507–511.
(16) Coleman, K. S.; Bailey, S. R.; Fogden, S.; Green, M. L. H. *J. Am. Chem. Soc.* **2003**, *125* (29), 8722–8723.
(17) Jiang, K. Y.; Eitan, A.; Schadler, L. S.; Ajayan, P. M.; Siegel, R. W.; Grobert, N.; Mayne, M.; Reyes-Reyes, M.; Terrones, H.; Terrones, M. *Nano Lett.* **2003**, *3* (3), 275–277.
(18) Liu, L.; Wang, T. X.; Li, J. X.; Guo, Z. X.; Dai, L. M.; Zhang, D. Q.; Zhu, D. B. *Chem. Phys. Lett.* **2003**, *367* (5−6), 747–752.
(19) Ou, Y. Y.; Huang, M. H. *J. Phys. Chem. B* **2006**, *110* (5), 2031–2036.
(20) Olek, M.; Hilgendorff, M.; Giersig, M. *Colloids Surf., A* **2007**, *292* (1), 83–85.
(21) Gao, C.; Li, W. W.; Jin, Y. Z.; Kong, H. *Nanotechnology* **2006**, *17* (12), 2882–2890.

10.1021/cm802648m CCC: $40.75
Published on Web 01/23/2009

the in situ growth of nanocrystals on CNTs,[4,22−25] chemical reduction reactions,[26,27] electrostatic-force-directed assembly,[28] and electrodeposition[29,30] reactions. Many of these distinctive methods for conjugation of nanoparticles to functionalized CNTs have been recently reviewed.[31] Nonetheless, a key disadvantage of direct formation of nanoparticles onto CNT surfaces has been the difficulty in defining and controlling the spatial coverage and distribution of nanocrystals. In fact, the in situ chemical synthesis of semiconductor nanoparticles directly onto the surfaces of carbon nanotubes usually leads to the generation of structures, which are highly polydisperse and inhomogeneous in shape and size.[32] The point therefore is to create well-defined heterostructure junctions that possess predictable chemistry and morphology.

Moreover, although the coating of presynthesized nanoparticles on CNT surfaces via noncovalent interactions, such as $\pi-\pi$ stacking interactions, is attractive in that it can theoretically preserve the intrinsic properties of CNTs, the associated presence of either a polymer or polyelectrolyte capping shell may actually shield or otherwise distort the inherent and often favorable functionality intrinsic to the nanoparticles or nanocrystals attached to them. For instance, the presence of a polyvinylpyridine (PVP) stabilizer on Pd nanoparticles has been known to decrease the catalytic efficiency of these nanoparticles in the Suzuki reaction.[33] In addition, this strategy is particularly problematic if one intends to rationally build more complicated nanotube−nanocrystal architectures composed of two or more different types of nanocrystals attached to the nanotube template.

In this work, therefore, we focus on covalent strategies to synthesize such complex CNT−nanoparticle heterostructures. There are several advantages to this particular approach. First, the shape and size of individual nanoparticles or nanocrystals can be easily tailored by sophisticated synthesis methods prior to combination with CNTs, thereby avoiding the influence of CNTs on the nucleation and growth processes of either nanoparticles or QDs. Second, covalent bonds can rigidly connect the linker molecules and CNTs in a reliable and robust manner, such that the nanoparticles will not become easily dislodged even after either sonication or extensive washing. Third, the spatial coverage and exact positions of either nanoparticles or nanocrystals depend on the precise nature of the chemical functionalities on the CNT surfaces, and these can be governed by controlling oxidation treatments and/or chemical reaction conditions.

Moreover, to the best of our knowledge, very little has been published on the covalently inspired fabrication of CNT-based nanocomposites containing two or more different types of nanocrystals. These structures are fascinating because of their potential for multifunctionality. Because precise manipulation, placement, and organization of nanoscale building blocks represent a key goal of nanoscience, in the context of this paper, this implies a predictable site-specific functionalization of CNTs with two or more different types of nanoparticles. A few studies have previously examined this idea of selective functionalization of CNTs. For instance, by making use of sidewall protection using a polystyrene matrix, selective bifunctionalization of the ends of CNTs with carboxylate groups at one end and thiol groups at the other was elegantly demonstrated.[34] In addition, a combination of focused-ion-beam (FIB) irradiation and subsequent mild chemical treatments was used to specifically anchor nanoparticles, fluorescent nanospheres, amino acids, as well as charge transfer proteins through electrostatic and covalent interactions directly onto these pretreated sites on the CNT surface.[35] Finally, the use of biological specific recognition strategies, involving small, amphiphilic proteins such as hydrophobins and their genetically engineered variants, has been proposed as a means to create hybrid nanostructures of CNTs and Au nanoparticles.[36]

Although all of these methods clearly offer a viable route forward, it is also evident that a more rigorous and quantifiable correlation between chemical treatment and attachment strategy of nanoparticles/QDs onto CNT surfaces would be very helpful. Indeed, in this paper, we seek to develop such a protocol, that would be neither tedious nor expensive, and would involve the use of ambient experimental conditions, if at all possible, without having to resort to either electric or magnetic fields or even expensive instrumentation. To the best of our knowledge, such a generalized, universal approach to site-selective placement of both nanoparticles and quantum dots, i.e., either at the ends or sidewalls of nanotubes, using simple chemistry, has not as yet been reported. As such, our work is highly relevant not only from the fundamental idea of tailoring chemical groups and moieties on nanotubes through a targeted protocol but also from the practical notion of using the nanotube surface as a platform with which to deterministically add specific functionalities and, therefore, particularly desirable attributes.

In this work, because of our prior experience with this system, we have used multiwalled carbon nanotubes (MWNTs) as a model template with which to construct complex hierarchical assembles of nanotube-nanocrystal heterostructures. That is, building on prior studies,[24] we

(22) Lee, Y.; Song, H. J.; Shin, H. S.; Shin, H. J.; Choi, H. C. *Small* **2005**, *1* (10), 975–979.
(23) Banerjee, S.; Wong, S. S. *Chemical Communications* **2004**, (16), 1866–1867.
(24) Banerjee, S.; Wong, S. S. *J. Am. Chem. Soc.* **2003**, *125* (34), 10342–10350.
(25) Banerjee, S.; Wong, S. S. *Adv. Mater.* **2004**, *16* (1), 34–37.
(26) Wang, D.; Li, Z. C.; Chen, L. W. *J. Am. Chem. Soc.* **2006**, *128* (47), 15078–15079.
(27) Zhang, R. Y.; Wang, X. M. *Chem. Mater.* **2007**, *19* (5), 976–978.
(28) Lu, G. H.; Zhu, L. Y.; Wang, P. X.; Chen, J. H.; Dikin, D. A.; Ruoff, R. S.; Yu, Y.; Ren, Z. F. *J. Phys. Chem. C* **2007**, *111* (48), 17919–17922.
(29) Guo, D. J.; Li, H. L. *J. Electroanal. Chem.* **2004**, *573* (1), 197–202.
(30) Quinn, B. M.; Dekker, C.; Lemay, S. G. *J. Am. Chem. Soc.* **2005**, *127* (17), 6146–6147.
(31) Georgakilas, V.; Gournis, D.; Tzitzios, V.; Pasquato, L.; Guldi, D. M.; Prato, M. *J. Mater. Chem.* **2007**, *17* (26), 2679–2694.
(32) Hu, J. P.; Shi, J. H.; Li, S. P.; Qin, Y. J.; Guo, Z. X.; Song, Y. L.; Zhu, D. B. *Chem. Phys. Lett.* **2005**, *401* (4−6), 352–356.
(33) Narayanan, R.; El-Sayed, M. A. *J. Am. Chem. Soc.* **2003**, *125* (27), 8340–8347.
(34) Chopra, N.; Majumder, M.; Hinds, B. J. *Adv. Funct. Mater.* **2005**, *15* (5), 858–864.
(35) Raghuveer, M. S.; Kumar, A.; Frederick, M. J.; Louie, G. P.; Ganesan, P. G.; Ramanath, G. *Adv. Mater.* **2006**, *18* (5), 547–552.
(36) Kurppa, K.; Jiang, H.; Szilvay, G. R.; Nasibulin, A. G.; Kauppinen, E. L.; Linder, M. B. *Angew. Chem., Int. Ed.* **2007**, *46* (34), 6446–6449.

Scheme 1. Synthetic Route Associated with the Preparation of MWNTs Coupled with (i) Thiol Groups, (ii) Au Nanoparticles (large orange spheres), and (iii) AET-Modified CdSe Nanocrystals (small red spheres)

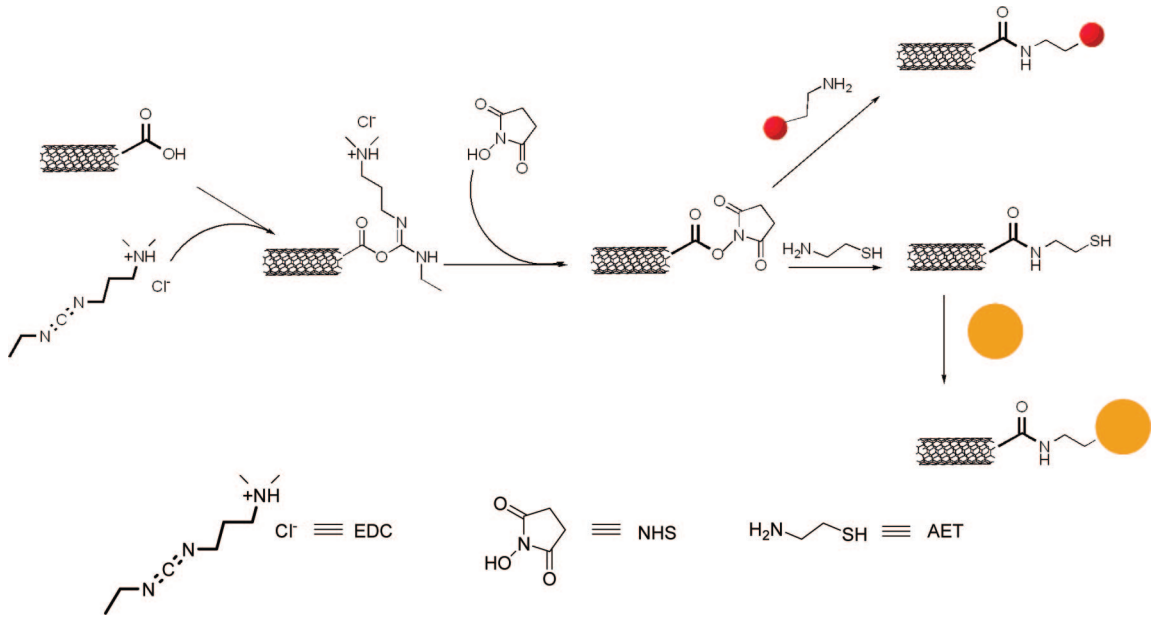

initially covalently functionalized our CNTs with carboxylic groups and then coated the oxidized MWNT surfaces with either preformed Au nanoparticles or CdSe QDs. The key step forward was that we could skew the positions and densities of these nanoparticles and QDs through appropriate variations in oxidation treatments and overall reaction conditions. That is, whereas conventional strategies tend to concentrate nanocrystals at the ends of MWNTs, where the largest concentration of carboxylic groups is naturally expected,[1] we have been able to obtain greater flexibility in the spatial placement of QDs and nanoparticles on our MWNT surface with appropriate variations in oxidative treatments and overall reaction conditions. For instance, one structure we have produced consists of Au nanoparticles localized at carbon nanotube tips with an overcoating of QDs along the sidewalls. We can also form the converse structure, consisting of QDs immobilized at the tips and Au nanoparticles concentrated along the sidewalls. Most importantly, we have been numerically rigorous in our analysis, quantifying our results on the basis of our electron microscopy data.

Why the emphasis on the precise synthesis of 0D−1D heterostructures? The properties of the assembled 0D−1D composite system are distinctly different from the simple sum of its parts. A significant observation from our laboratory has been the quenching of luminescence emission from the quantum dot when in close proximity to the nanotube.[1] This suggests the feasibility of rapid energy transfer to the nanotube. This phenomenon seems to depend mainly on the relative separation of the nanotube and quantum dot as it has been observed with chemical linkers,[1,37] direct sidewall growth,[24] and polymer spacers.[38] However, it is interesting to note that in cases where an inorganic dielectric layer was used to either cap the nanotube or the QD, the fluorescence is recovered.[39] In general, there seems to be only a weak perturbation of the intrinsic electronic states of either system, as absorption measurements have shown little or no shifts in the electronic transition energies.[37] As it appears that the electronic coupling between the 0D and 1D systems is weak, the likely mechanism for fluorescence quenching then involves either electron transfer or resonance energy transfer between the two systems or a combination of these processes. Both electron transfer and energy transfer have been shown to be important in natural photosynthetic systems and to possess distinctive length, time, and energy scales.[40]

2. Experimental Section

The preparation, thiolation, and oxidation of MWNTs as well as Au and CdSe quantum dots are well-known protocols and our slight variations on these procedures are described in the Supporting Information section. Herein, we focus on methodologies for effective heterostructure generation.

2.1. Heterostructure Formation. We should note that in all of these protocols, the reactions were carried out on sub-microgram quantities of starting materials, and hence overall yields for each of the as-prepared heterostructures were not determined.

2.1.1. Synthesis of MWNT−Au Conjugates. One-tenth of a milligram of thiolated MWNTs was dispersed in ∼1 mL of distilled water by sonication. As described in Scheme 1, an aqueous solution of Au nanoparticles (NPs) was then added to the above solution and incubated for 2 h to promote gold−thiol bond formation. The final concentration of Au NPs in solution was 100 nM. The solution was subsequently filtered and washed with an excess of water.

2.1.2. Synthesis of MWNT−Au−CdSe Conjugates. Prior to reaction with CdSe, 0.1 mg of MWNT−Au conjugates were further oxidized in 1 M HNO_3 for 0.5, 1, 6, 12, and 24 h in separate experiments, after which they were extensively washed with distilled water, oven-dried, and redispersed in distilled water. An aliquot of

(37) Haremza, J. M.; Hahn, M. A.; Krauss, T. D. *Nano Lett.* **2002**, *2* (11), 1253–1258.
(38) Grzelczak, M.; Correa-Duarte, M. A.; Salgueirino-Maceira, V.; Giersig, M.; Diaz, R.; Liz-Marzan, L. M. *Adv. Mater.* **2006**, *18* (4), 415–420.
(39) Ravindran, S.; Chaudhary, S.; Colburn, B.; Ozkan, M.; Ozkan, C. S. *Nano Lett.* **2003**, *3* (4), 447–453.
(40) Noy, D.; Moser, C. C.; Dutton, P. L. *Biochim. Biophys. Acta, Bioenerg.* **2006**, *1757* (2), 90–105.

Scheme 2. Possible Mechanisms and Strategies for the Synthetic Formation of MWNT Conjugates Containing Both CdSe Nanocrystals (small red spheres) and Au Nanoparticles (large orange spheres)

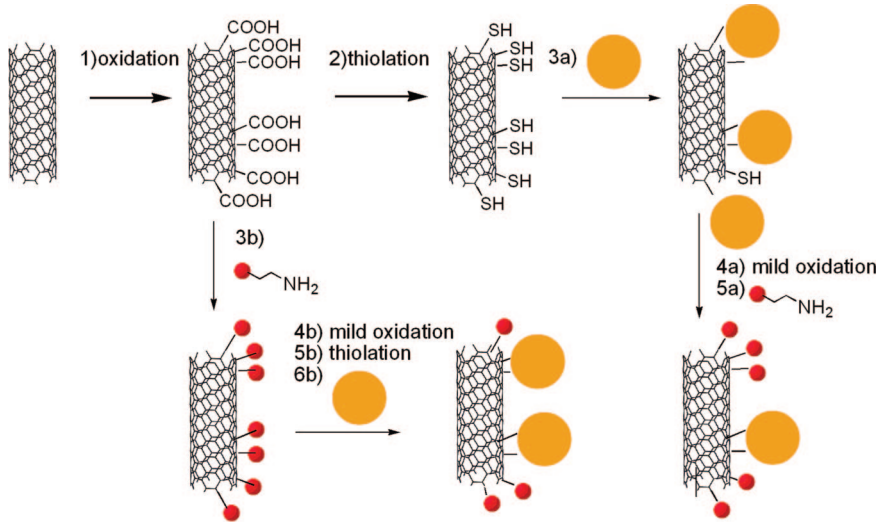

0.1 M MES (2-(*N*-morpholino) ethanesulfonic acid) buffer (pH 6.0), EDC (1-ethyl-3-(3-dimethylaminopropyl) carbodiimide), and NHS (*N*-hydroxysuccinimide) in aqueous solution was then added to the above acid-treated MWNT−Au conjugates to activate these structures for further coupling with aminoethanethiol-derivatized cadmium selenide, (AET−CdSe), as highlighted in Scheme 2. The solution was stirred for 2 days. The resulting material was subsequently filtered and washed to remove loosely bound aggregates.

2.1.3. Synthesis of MWNT−CdSe Conjugates. One-tenth of a milligram of oxidized MWNTs was dispersed in ∼1 mL distilled water by sonication. As shown in Scheme 1, an aliquot of 0.1 M MES buffer (pH 6.0), EDC and NHS aqueous solution was added to the above solution, followed by the addition of AET−CdSe. The solution was stirred for 2 days.

2.1.4. Synthesis of MWNT−CdSe−Au Conjugates. One-tenth of a milligram of MWNT−CdSe conjugates were further oxidized in 1 M HNO_3 for 0.5, 1, 6, 12, and 24 h in separate experiments, followed by extensive washing with distilled water and oven drying. The subsequent thiolation of acid-treated MWNT−CdSe conjugates was identical to what was reported in the Supporting Information section to create active sites for coupling with Au NPs, as illustrated in Scheme 2. Specifically, an aqueous solution of Au nanoparticles was added to a dispersed suspension of thiolated MWNT−CdSe and subsequently incubated for 2 h. The resulting material was subsequently filtered and washed to remove loosely bound aggregates.

3. Characterization

The resulting products were characterized by means of X-ray diffraction (XRD), Fourier transform infrared spectroscopy (FT-IR), transmission electron microscopy (TEM), ultraviolet−visible (UV−visible) spectroscopy, and photoluminescence spectroscopy (PL).

X-ray Diffraction. Crystallographic and purity information on nanotube-nanocrystal heterostructures were obtained using powder XRD. To analyze these materials, we subsequently sonicated as-prepared samples and dispersed them in ethanol for about 2 min, and finally air-dried them upon deposition onto glass slides. Diffraction patterns of these materials were collected using a Scintag diffractometer, operating in the Bragg configuration using Cu Kα radiation (λ = 1.54 Å) from 20 to 80° at scanning rates of 0.25° per min.

Electron Microscopy. Diameters and lengths of as-prepared nanostructures were initially characterized using a field emission scanning electron microscopy instrument (FE-SEM Leo 1550), operating at an accelerating voltage of 2.0 kV and equipped with energy-dispersive X-ray spectroscopy (EDS) capabilities. Samples for SEM were prepared by dispersing as-prepared nanostructures in ethanol, sonicating for about 2 min, and then depositing the sample onto either a copper grid or a silicon wafer, attached to a SEM brass stub.

Low-magnification TEM images were taken at an accelerating voltage of 80 kV on a FEI Tecnai12 BioTwinG^2 instrument, equipped with an AMT XR-60 CCD Digital Camera System. High-resolution images were obtained on a JEOL 2010F instrument, equipped with an INCA EDS system, at accelerating voltages of 200 kV. Specimens for all of these TEM experiments were prepared by dispersing the as-prepared product in ethanol, sonicating it for 2 min to ensure adequate dispersion of the nanostructures, and dipping one drop of solution onto a 300 mesh Cu grid, coated with a lacey carbon film.

Optical Spectroscopy. FT-mid-IR data were obtained on a Nexus 670 (Thermo Nicolet) equipped with a single reflectance zinc selenide (ZnSe) ATR accessory, a KBr beam splitter, and a DTGS KBr detector. Solid samples were placed onto a ZnSe crystal. Measurements were obtained in absorbance mode using the Smart Performer module. UV−visible spectra were collected at high resolution using a Thermospectronics UV1 with quartz cells maintaining a 10 mm path length. Samples were prepared by sonication in distilled water. Data were corrected to account for the solvent background.

Photoluminescent Activity. Samples for photoluminescence (PL) spectra were initially dispersed in deionized water and sonicated for 2 min. Fluorescence data were obtained at room temperature on a Jobin Yvon Spex Fluorolog 3 with a 1 s integration time. PL spectra were taken using excitation wavelengths of 400 nm.

4. Basis of Calculations

Commercial pristine MWNTs measured 16.3 ± 5.1 nm in diameter and ∼1−5 μm in length. As a rough guide to the extent of functionalization, which is an important factor in our experiments, we approximated the tips and sidewalls of the CNTs as hemispheres and cylinders, respectively, whose intrinsic structure was reasonably assumed to have remained relatively intact during the entire functionalization process. Our calculations showed that for the dimensional range encompassed by our samples, the surface area

ratio of tips to that of sidewalls spanned from 1:122 to 1:613, reinforcing the logical conclusion that the accessible reactive surface area available to the nanoparticles was considerably higher along the nanotube sidewalls than at the tips. The numbers of nanoparticles localized at the tips and sidewalls of the tubes were separately counted from among 20 different tubes for each treated MWNT−nanoparticle conjugate. In this work, we characterize the nature of our heterostructures using a number of different parameters. For instance, the percentage of nanoparticles at the tips was obtained by dividing the number of nanoparticles at the tips by the total number of nanoparticles on the entire CNT surface. By analogy, the percentage of nanoparticles along the sidewalls could also be computed by dividing the number of nanoparticles along the nanotube sidewalls by the total number of nanocrystals on the entire CNT surface. The average coverage of nanoparticles of each MWNT−nanoparticle conjugate was noted by dividing the total number of nanoparticles attached to the CNT surface by the corresponding length of the MWNTs in microns. For practical purposes, because of the high surface area along the sidewalls of CNTs as compared with that at the tips, we could reasonably ignore the latter quantity in our overall nanocrystal/nanoparticle density computation.

5. Results and Discussion

Characterization data on the synthesis of Au nanoparticles, the ligand exchange of CdSe quantum dots, oxidation of MWNTs, and thiolation of MWNTs are extensively described in the Supporting Information section (including Figures S1−S7). Again, we will focus on the nanocrystal−nanotube heterostructure generation herein.

5.1. Synthesis of MWNT−Au Conjugates. Oxidized MWNTs were treated with an EDC/NHS conjugate so as to facilitate subsequent formation of amide bonds onto the oxygenated sites of the processed MWNTs and thereby enhance overall reaction efficiency specifically with Au nanoparticles. Scheme 1 highlights a plausible synthesis process scheme associated with CNT functionalization with thiol groups, so as permit successful attachment of gold nanoparticles onto the nanotube surface.

TEM images illustrated in Figure 1B−F showed the presence of a series of MWNT−Au conjugates, prepared using different oxidation treatments from relatively mild wet air to comparatively stronger acid treatments. High-resolution TEM images showed the successful formation of MWNT−Au conjugates, wherein Au nanoparticles were bound to MWNTs along the sidewall (images A and B in Figure 2). Lattice fringes associated with Au nanoparticles as well as the interface between the nanoparticles and the MWNT surface were clearly discernible. Similarly, well-defined lattice fringes corresponding to CdSe nanocrystals were also observed in MWNT−CdSe conjugates, as shown in C and D in Figure 2. The results (shown in Table 1) confirmed that the degree of immobilization of Au nanoparticles on the tube surface strongly correlated with the nature of the oxidative treatment.[23,41,42] For instance, the control experiment in which Au nanoparticles were incubated with unoxidized MWNTs under exactly identical conditions

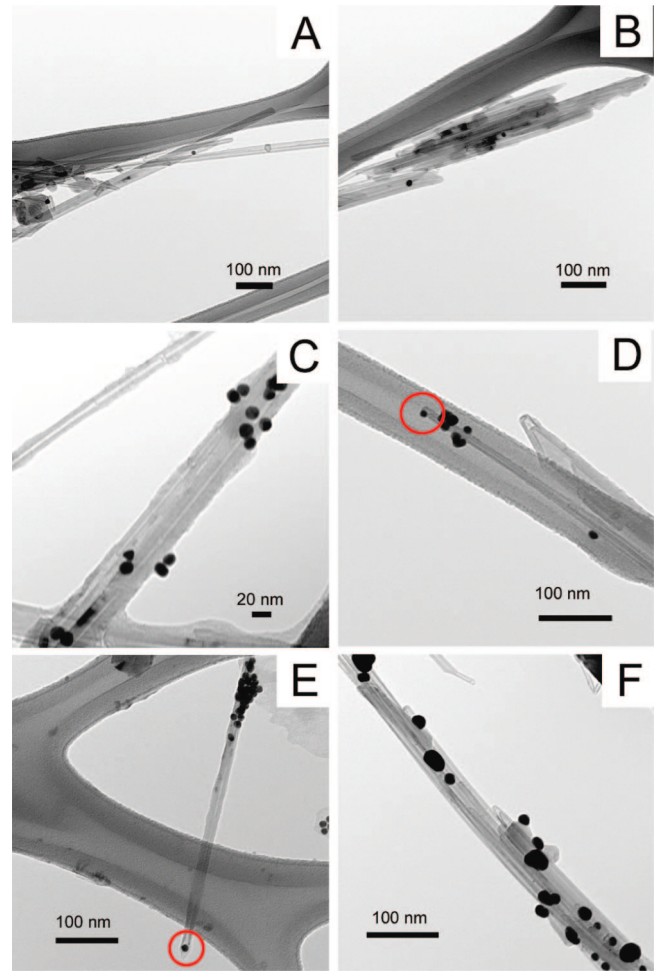

Figure 1. (A) TEM images of unoxidized MWNTs incubated with Au nanocrystals. MWNT−Au conjugates generated after various different oxidation treatments: (B) wet air, (C) ozonolysis, (D) 9 M HNO_3, (E) $KMnO_4/H_2SO_4$, and (F) H_2SO_4/ HNO_3. Red circles highlight locations of Au nanoparticles anchored at the tips of carbon nanotubes.

suggested no obvious attachment of Au NPs (Figure 1A), indicating a weak noncovalent interaction between Au NPs and MWNTs. We also found that the MWNT−Au conjugate originating from wet air treatment (Figure 1B) possessed the lowest surface coverage of Au NPs (1.0 particle/μm) because of its relatively low extent of oxidation.

Because of the relatively larger diameter of the outer walls of MWNTs and hence smaller in-plane strain in the graphite sheets as compared with that of SWNTs, a harsher oxidative regime is required to attack MWNT surfaces for the purposes of functionalization.[39,43] Not surprisingly, as seen in Figure 1F and Table 1, H_2SO_4/HNO_3-treated MWNTs possessed a relatively high density of functional groups and hence the highest density of Au nanoparticles (20.3 particles/μm) observable on the nanotube surface. By contrast, we found only an average of 12.0 nanoparticles of Au/μm for a slightly milder oxidative treatment such as the use of 9 M nitric acid (Figure 1D) alone. It is worth noting that although the statistical error on some of our measurements was relatively high, partly because of polydispersity in nanotube length and diameter, the trend of Au nanoparticle coverage on the

(41) Li, X. H.; Niu, J. L.; Zhang, J.; Li, H. L.; Liu, Z. F. *J. Phys. Chem. B* **2003**, *107* (11), 2453–2458.
(42) Zhang, J.; Zou, H. L.; Qing, Q.; Yang, Y. L.; Li, Q. W.; Liu, Z. F.; Guo, X. Y.; Du, Z. L. *J. Phys. Chem. B* **2003**, *107* (16), 3712–3718.
(43) Brukh, R.; Mitra, S. *J. Mater. Chem.* **2007**, *17* (7), 619–623.

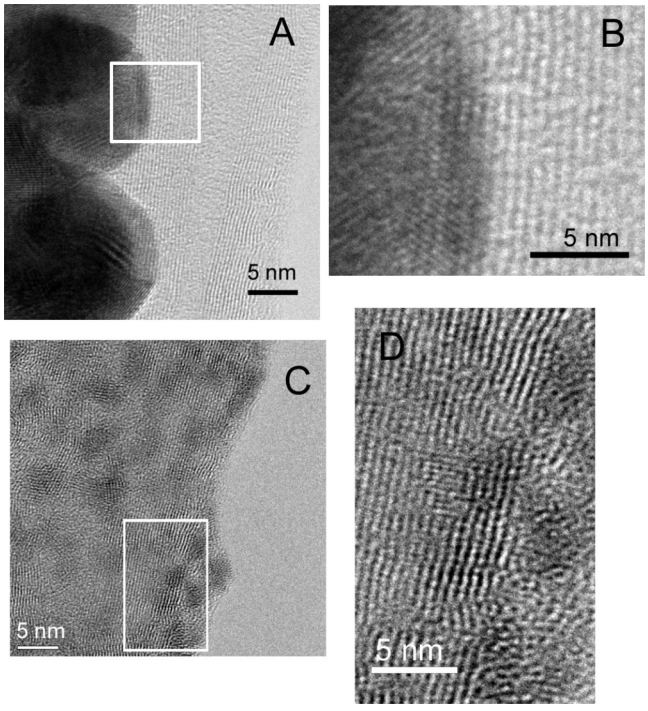

Figure 2. High-resolution TEM image of either (A) Au or (C) CdSe nanocrystals bound onto the surface of MWNTs. (B) Magnified image of the area indicated by the square in (A). (D) Magnified image of the area outlined by the square in (C).

MWNT surface clearly correlated with the strength of the oxidation treatment.

Other factors are likely at work in accounting for our observations. For example, it is reasonable to assume that the solubility of CNTs, as defined by its chemical treatment, in the reaction media also affected the subsequent coverage of nanoparticles noted. In this study, for instance, Au nanoparticles were incubated with thiolated MWNTs in aqueous solution. The nature of pristine CNTs is hydrophobic. In that case, a poor dispersion of these CNTs in solution would have hampered the diffusion of nanoparticles into the crevices and interstitial spaces separating individual as well as bundles of CNTs, and hence, there would have been a smaller contact area or reaction surface for the nanoparticles. By contrast, the high concentration of carboxylic groups on the surface of highly oxidized CNTs induced by the strong oxidation process renders these modified MWNTs far more hydrophilic and more soluble in the reaction medium, which, in turn, leads to a greater probability of interaction with Au nanoparticles.

5.1.1. Spatial Distribution of Nanoparticle Coverage Correlates with Strength of Oxidative Method. It is obvious that the spatial coverage of Au nanoparticles on the nanotube surface correlates strongly with the nature of the oxidative treatment, as shown in Table 1. For instance, it has been proposed that the mechanism of ozonolysis of CNTs involves ozone addition to the conjugated double bonds of the outer CNT circumference through a facile 1,3-dipolar cycloaddition reaction.[44] Therefore, one would theorize that the distribution of oxygenated functional groups would favor a higher density of Au nanoparticles along the sidewalls of CNTs as compared with that at the tips. In fact, this was borne out by experimentation (Figure 1C) in which there was a very strong propensity for Au nanoparticles (92.4%) to attach to the nanotube sidewall. Moreover, this result was consistent with and serves as confirmation for the notion that ozonolysis is a rational means for derivatizing SWNT sidewalls, as initially proposed.[44]

By analogy, selective introduction of oxygenated groups such as carboxylic groups onto the ends of CNTs with either minimal or no damage to the sidewalls can be theoretically achieved by carefully choosing different oxidation protocols. For instance, acid oxidation treatments are thought to selectively open the end caps of MWNTs as well as to etch away at the tube's sidewalls and defect sites, thereby coating the nanotubes with keto, carboxylic, aldehyde, and alcoholic groups.[45,46] The reason is that the end caps of MWNTs are considerably more reactive than the sidewalls because of the higher intrinsic strain of the pentagonal rings, and thus, these sites ought to be more easily attacked by oxidants as opposed to the tube sidewalls. In the current work, as we expected, the use of 9 M nitric acid reflux at 50 °C preferentially and selectively oxidized MWNTs at their ends (30.9%). The increased localization of carboxylic acid groups enabled the anchoring and coordination of the highest density of Au nanoparticles at the MWNT tips as compared with any other treatment method studied herein. This observation is highlighted in Figure 1D, where the red circle corresponds to Au nanoparticles anchored at the tips of the carbon nanotubes.

By contrast, a stronger acid treatment, such as a combined $KMnO_4$ /H_2SO_4 treatment, not only introduced reactive acid groups at the ends of the CNTs (Figure 1E) but also had the unintended side effect of enhancing the level of defect sites along the tube sidewalls. Consequently, in this case, the probability of attachment of Au nanoparticles along the sidewalls increased to 86.8% as compared with 69.1% for 9 M HNO_3 treated MWNTs. Using a similar argument, a combined H_2SO_4/HNO_3 treatment with prolonged oxidation followed by sonication nondiscriminately and aggressively attacked the entire CNT surface, creating a large number of defect sites not only at the ends but also along the sidewalls (Figure 1F). In fact, this harsh protocol not only led to the highest percentage of Au nanoparticles that we were able to experimentally achieve along the sidewalls of the MWNTs (94.6%) but also the highest overall density observed (20 particles/μm).

Interestingly, when a considerably milder acid treatment (i.e., 3 M HNO_3 at 50 °C) as well as wet air oxidation was used, the percentage of Au nanoparticles at the tips unexpectedly decreased. As mentioned above, the relatively poor hydrophilicity of notably mildly processed MWNTs in the reaction medium is a key complicating factor in influencing the nature of nanoparticle attachment. Thus, a high degree of aggregation and bundling of relatively poorly solvated

(44) Banerjee, S.; Wong, S. S. *J. Phys. Chem. B* **2002**, *106* (47), 12144–12151.

(45) Liu, J.; Rinzler, A. G.; Dai, H. J.; Hafner, J. H.; Bradley, R. K.; Boul, P. J.; Lu, A.; Iverson, T.; Shelimov, K.; Huffman, C. B.; Rodriguez-Macias, F.; Shon, Y. S.; Lee, T. R.; Colbert, D. T.; Smalley, R. E. *Science* **1998**, *280* (5367), 1253–1256.

(46) Hiura, H.; Ebbesen, T. W.; Tanigaki, K. *Adv. Mater.* **1995**, *7* (3), 275–276.

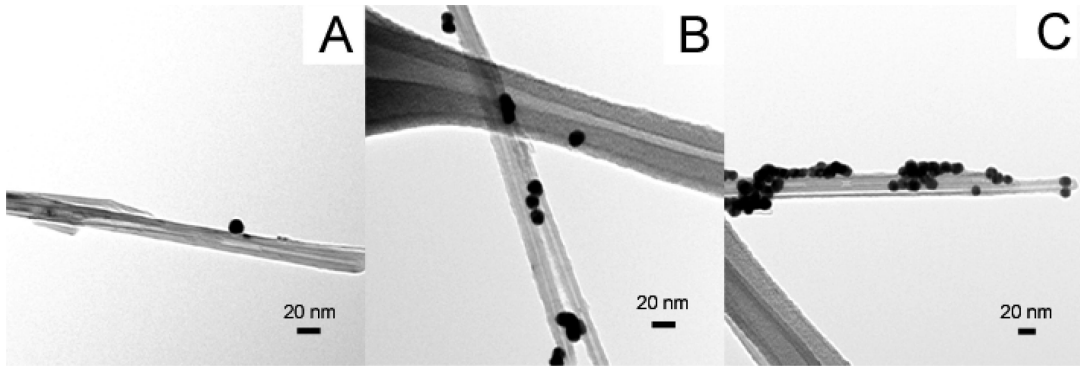

Figure 3. Probing the effect of nanocrystal concentration. TEM images of MWNT−Au conjugates incubated with a concentration of Au nanoparticles set at (A) 50, (B) 100, and (C) 200 nM. Constant incubation time: 2 h. MWNTs were initially oxidized with H_2SO_4/HNO_3.

Table 1. Spatial Distribution and Coverage of Au Nanoparticles on CNT Surfaces Subjected to Different Oxidation Treatments

MWNT−Au conjugates	oxidation treatment	percentage of nanocrystals along sidewall (%)	percentage of nanocrystals at the tips (%)	overall density of nanocrystals (μm^{-1})
0	unoxidized			0
1	wet air	100	0	1.0 ± 0.5
2	ozonolysis/H_2O_2	92.4	7.6	7.8 ± 3.0
3a	3 M HNO_3 at 50 °C	90.9	9.1	6.9 ± 3.1
3b	9 M HNO_3 at 50 °C	69.1	30.9	12.0 ± 2.4
4	$KMnO_4$/ H_2SO_4	86.8	13.2	12.7 ± 4.4
5	H_2SO_4 /HNO_3	94.6	5.4	20.3 ± 8.5

Table 2. Spatial Distribution and Coverage of Au Nanoparticles with Different Nanoparticle Concentrations on Carbon Nanotube Templates[a]

concentration of Au nanoparticles (nM)	percentage of nanoparticles along the sidewall	percentage of nanoparticles at the tips and ends	density coverage of nanoparticles on MWNTs (μm^{-1})
50	100	0	1.0 ± 0.5
100	94.6	5.4	20.3 ± 8.5
200	98.0	2.0	48.0 ± 6.9

[a] Data were obtained from MWNT−Au conjugates, in which MWNTs were initially oxidized by H_2SO_4/HNO_3.

MWNTs in these specific cases likely increased the degree of steric hindrance associated with nanoparticle accessibility to the reactive sites on the CNT surface. As such, individual nanotube tips may not have been as adequately exposed to the presence of Au nanoparticles, thereby dramatically reducing reactivity at these end sites as compared with the sidewalls and hence leading to the <10% values of observed loading.

5.1.2. Observed Nanoparticle Coverage Depends on Precursor Particle Concentration. We probed the effect of increasing nanoparticle concentration on the resultant density of particle coverage. Thiolated MWNTs, which had been initially oxidized by a H_2SO_4/ HNO_3 treatment, were incubated with successively higher concentrations of Au nanoparticles present at 50, 100, and 200 nM for 2 h. As expected and shown in Figure 3 and Table 2, a successively higher particle concentration incubated with MWNTs yielded a correspondingly higher achievable density (up to 48.0 particles/μm) of Au nanoparticles. On the other hand, the actual spatial distribution of nanocrystals at the ends, defect sites, and sidewalls was not noticeably affected by changes in the concentration of Au nanoparticles. One could make the case, however, that the defect sites along the sidewalls were initially coordinated with reactive, incoming nanocrystals followed by subsequent reaction at the ends.

5.1.3. Increasing Incubation Time Yields Higher Nanoparticle Coverages. To determine the effect of incubation time on overall nanocrystal coverage on nanotube surfaces, we tested CdSe and Au nanocrystals in the presence of oxidized MWNTs and thiolated MWNTs, respectively. H_2SO_4/HNO_3-treated MWNTs were incubated with AET−CdSe nanocrystals for different incubation/reaction times of 0.5, 2, and 48 h with a constant CdSe concentration of 100 nM. In the resulting MWNT−CdSe conjugates, the density of QDs increased significantly from a low of ~0 particles/μm on the CNT surface to 71.3 particles/μm upon increasing incubation times from 0.5 to 48 h (Figure 4 and Table 3). By contrast, for the fabrication of MWNT−Au conjugates, in which the MWNTs were oxidized by 9 M HNO_3 and the concentration of added Au nanoparticles was 100 nM, the coverage density remained relatively stable at about 12−14 particles/μm over the entire incubation time range from 0.5 to 48 h (Table 4).

It is worth noting that even though the MWNTs in these two types of nanotube−particle conjugates were modified by different oxidation treatments, that fact alone likely cannot fully explain the clear difference in reactivity between the two conjugates. That is, the difference in particle attachment rates may also be a reflection of the fact that these two types of conjugates were created by distinctive chemistries. Specifically, in the MWNT−CdSe conjugate system (step 3b, Scheme 2), the attachment rate was determined by the rate of amide bond formation between carboxylic acids on the MWNT and amine groups on the CdSe, whereas creation of Au−S bonds governed the production of thiolated MWNT−Au conjugates (Step 3a, Scheme 2). Partly because of bond strength considerations and kinetic rate constant data, it is

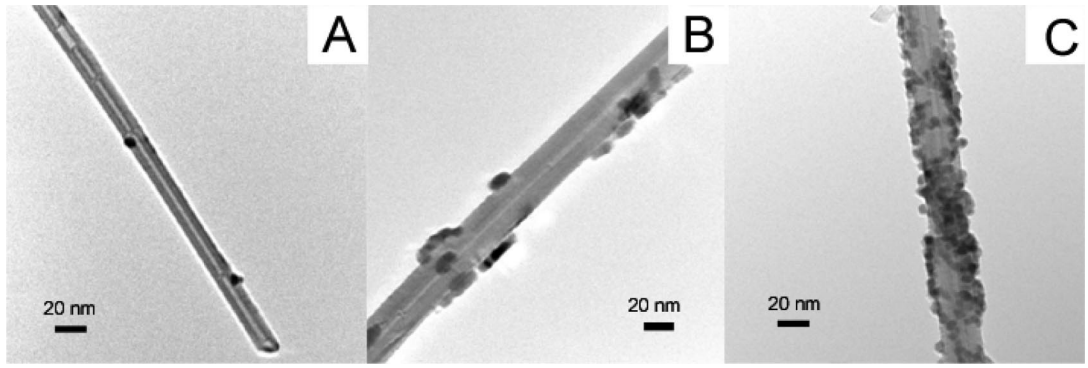

Figure 4. TEM images of MWNT−CdSe conjugates with incubation times of (A) 0.5, (B) 2, and (C) 48 h. Constant concentration of CdSe nanocrystals: 100 nM. MWNTs were initially oxidized using a H_2SO_4/HNO_3 treatment.

Table 3. Spatial Distribution and Coverage of CdSe Nanocrystals onto Carbon Nanotube Templates with Different Incubation Times[a]

incubation time (h)	percentage of nanocrystals along the sidewall	percentage of nanocrystals at the tips and ends	coverage of nanocrystals on MWNTs (μm^{-1})
0.5	100	0	1.0 ± 1.0
2	98.5	1.5	15.4 ± 13.7
48	96.6	3.4	71.3 ± 14.2

[a] Data were obtained from MWNT−CdSe conjugates, in which MWNTs were initially oxidized by H_2SO_4/HNO_3.

Table 4. Spatial Distribution and Coverage of Au Nanocrystals onto Carbon Nanotube Templates Processed with Different Incubation Times[a]

incubation time (h)	percentage of nanocrystals along the sidewall	percentage of nanocrystals at the tips and ends	coverage of nanocrystals on MWNTs (μm^{-1})
0.5	82.0	18.0	13.4 ± 3.4
2	69.1	30.9	12.0 ± 2.4
48	74.7	25.3	14.5 ± 3.8

[a] Data were obtained from MWNT−Au conjugates, in which MWNTs were initially oxidized by 9 M HNO_3.

known that the formation of Au−S bonds[47] is faster than that of amide bond production.[48]

More importantly, the MWNT−CdSe system showed a substantially greater coverage of QDs on the tubes (71.3 particles/μm) as compared with the MWNT−Au analogue (20.3 particles/μm) under similar reaction conditions. This observation could be ascribed to a higher diffusion of QDs through the MWNT framework, because of the relatively smaller size of these CdSe QDs permeating into the interstitial spaces between individual as well as bundles of CNTs. In addition, as shown in Scheme 2, it can be plausibly reasoned that in either case, there was a dense quantity of either thiol or carboxylic groups dangling at either the defect sites or the ends of the oxidized MWNTs.

Hence, in the case of MWNT−Au conjugates, the larger Au nanoparticles (12.7 nm) attached to the reactive CNT ends might have posed a steric hindrance factor and therefore, have potentially blocked additional nanoparticles from approaching and coordinating onto the remaining reactive thiol sites available on the CNT sidewall. By contrast, for MWNT−CdSe heterostructures, the relatively smaller size of the CdSe QDs used, measuring 4.2 nm, would ensure a more facile accessibility of these particles to reactive carboxylic groups coating the nanotube sidewalls, and therefore, a greater likelihood of generating a dense coating of QDs on its surface without a high degree of spatial impediment.

5.2. Hierarchical Synthesis of MWNT−Au−CdSe conjugates. To synthesize more sophisticated structures with different nanoparticles localized at the tips and sidewalls of the nanotubes, respectively, as-prepared MWNT−Au conjugates, using MWNTs previously treated with H_2SO_4/HNO_3, were used as the starting motif material. Specifically, it was noted that Au nanoparticles had the highest spatial preference for the tube sidewalls in that particular system as compared with analogous, oxidized MWNT-based Au heterostructures generated by other treatments. Moreover, the higher hydrophilicity of these specifically oxidized MWNTs likely enabled a better dispersability of the MWNTs in reaction solution, thereby increasing the probability of interaction between the tips of the MWNTs with the additional CdSe nanocrystal population.

Experimentally, as-prepared MWNT−Au conjugates were further oxidized in 1 M HNO_3 so as to create or "refresh" new defect sites as well as additional carboxylic groups, prior to incubation with CdSe. Energy-dispersive spectroscopy (EDS) used in conjunction with SEM confirmed the presence of Au NPs in the precursor MWNT−Au heterostructures (A and C in Figure 5) as well as the presence of both Au NPs and CdSe QDs in as-prepared MWNT−Au−CdSe conjugate products (B and D in Figure 5).

TEM images shown in Figure 6A−E highlight the formation of MWNT−Au−CdSe conjugates, prepared from MWNT−Au precursor templates, which had been initially oxidized with 1M HNO_3 for varying reaction times prior to incubation with Cdse. The red arrows denote the presence of Au NPs whereas the blue arrows indicate the location of CdSe QDs. It can be noted that upon prolonged reaction of the MWNT−Au precursor template in dilute acid, we gradually lost Au nanoparticle coverage on the CNT surface (Table 5) as the number of CdSe nanoparticles increased in the final MWNT−Au−CdSe product. That is, the measured density of Au NPs dropped from 20.3 particles/μm to approximately zero particles/μm within 24 h of acid oxidation of the MWNT−Au precursor, while the corresponding

(47) Liao, S.; Shnidman, Y.; Ulman, A. *J. Am. Chem. Soc.* **2000**, *122* (15), 3688–3694.
(48) Kouassi, G. K.; Irudayaraj, J. *J. Nanobiotechnol.* **2006**, *4* (8), 1–10.

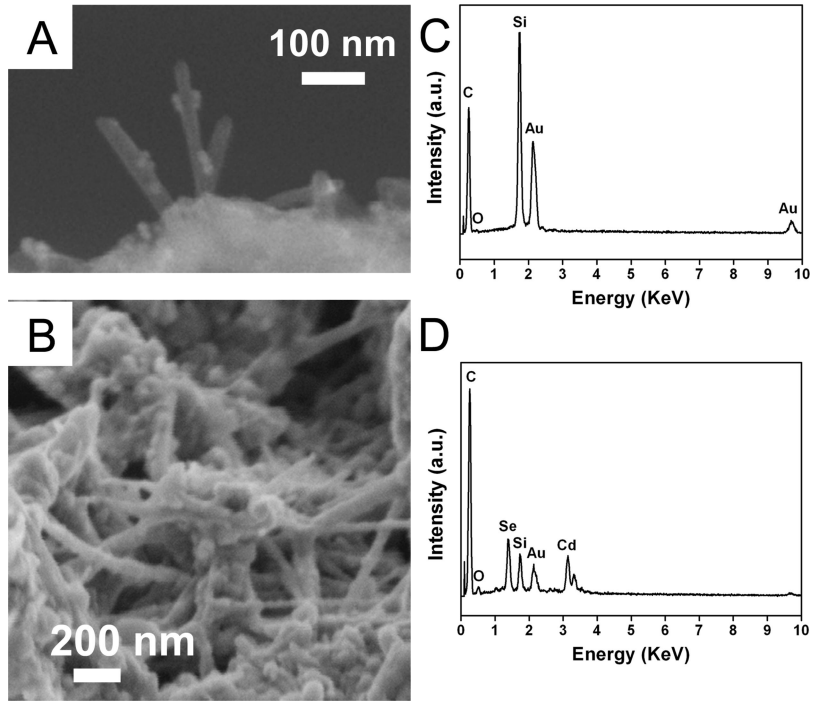

Figure 5. SEM images of (A) MWNT−Au conjugates and (B) MWNT−Au−CdSe conjugates. EDS of (C) MWNT−Au conjugates and (D) MWNT−Au−CdSe conjugates, in which MWNTs were oxidized by a HNO_3/H_2SO_4 treatment. The SEM samples were prepared on a silica matrix.

density of CdSe nanocrystals, which had been specifically incubated with these oxidized MWNT−Au samples, increased from essentially zero particles/μm to 50.9 particles/μm in the resulting MWNT−Au−CdSe product. By comparison, as a control experiment, MWNT−Au conjugates, which had been further oxidized for 24 h but not incubated with CdSe, are shown in Figure 6F. Our overall data suggest that it was predominantly the acid treatment as opposed to either any real displacement or exchange reaction with CdSe QDs that resulted in the loss of Au nanoparticles. In fact, our observations can be ascribed to two factors. First, although the use of dilute acid was necessitated in order to prevent excessive damage of preformed amide bonds, it is unlikely that all preformed amide bonds in our MWNT−Au conjugate precursor templates remained intact during the entire process, as amide bonds are easily hydrolyzed under either acidic or basic conditions. Second, it has been previously reported that dissociation of the thiol ligand from the surface of nanoparticles can be induced by lowering the pH of the reaction solution, as the added hydrogen ions compete for and displace the surface ligands associated with preattached nanoparticles,[49] resulting in the concomitant loss of Au nanoparticles from our CNTs in our specific case.

In Figure 7, as a function of increasing oxidation time of the MWNT−Au precursor template, the percentage of Au NPs in the resulting MWNT−Au−CdSe conjugate was found to decrease sharply due to a higher density of CdSe QDs coating the CNT surface. In order to understand this observation, we note the presence of two different sets of reactive sites on the nanotubes: (i) one group, which had been left unoccupied (and unreacted) by Au NPs in the precursor MWNT−Au conjugates prior to the 1 M HNO_3 oxidation step, and (ii) an additional group of sites, which continued to remain reactive as Au NPs were lost upon 1 M HNO_3 oxidation (Scheme 2, step 4a). Both sets of sites nonetheless provided for abundant locations at which CdSe QDs could be subsequently bound onto the surfaces of the CNTs (steps 4a and 5a in Scheme 2).

Overall, these results, as summarized in Table 5, demonstrated that the coverage of CdSe Qds in the resulting MWNT−Au−CdSe conjugate increased dramatically upon an oxidation time of 1 h of the initial MWNT−Au precursor template. Quantum dot coverage then leveled off, even after oxidative reaction times of 24 h of the conjugate precursor, suggesting a saturation of available reactive sites, previously occupied by but subsequently vacated by the original Au NPs. With respect to the spatial distribution of either NPs or QDs in the hierarchical product, the number of Au NPs at the tips of the final product gradually decreased with increasing oxidation time of the MWNT−Au precursor template. That observation was coupled with a concomitant increase of CdSe QDs on the resulting MWNT−Au−CdSe surface. A maximum level of up to 9.0% of total CdSe QD coverage was observed in a sample that had been incubated with a MWNT−Au template, subjected to a 1 h oxidation in the presence of nitric acid. Essentially, we observed that the majority of the tips of MWNTs ended up being occupied by CdSe QDs after their introduction into the reaction medium, whereas the remaining Au nanoparticles, still anchored on the MWNT surface, were primarily distributed along the MWNT sidewalls, as illustrated in Figure 6B. With increasing oxidation time of the MWNT−Au precursor template, Au NPs along the CNT sidewalls were continuously "replenished" with CdSe QDs, ultimately leading to

(49) Aldana, J.; Lavelle, N.; Wang, Y. J.; Peng, X. G. *J. Am. Chem. Soc.* **2005**, *127* (8), 2496–2504.

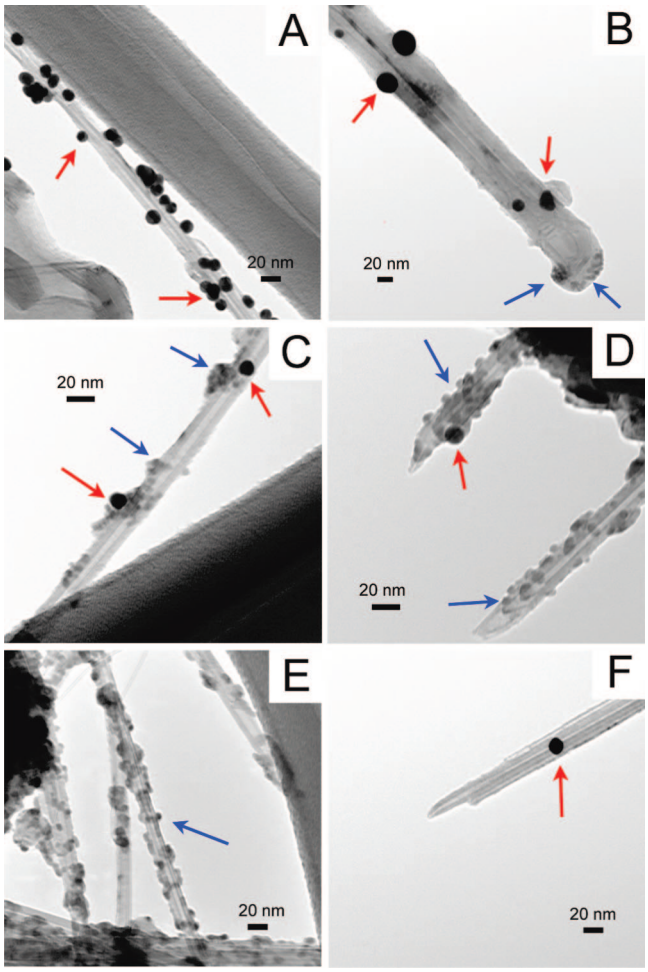

Figure 6. TEM images of MWNT−Au−CdSe conjugates. MWNT−Au conjugates were initially subjected to acid oxidation and subsequently reacted with AET−CdSe nanocrystals in the presence of EDC for 2 days. Results are shown for MWNT−Au−CdSe products generated from MWNT−Au precursor templates, previously oxidized in 1 M HNO_3 for (A) 0.5 h, (B) 1 h, (C) 6 h, (D) 12 h, and (E) 24 h. As a control, a (F) MWNT−Au conjugate is shown after 1 M HNO_3 oxidation for 24 h but without incubation with AET−CdSe nanocrystals. Starting MWNTs were initiallty oxidized using a H_2SO_4/HNO_3 treatment. The red arrows denote the presence of Au NPs whereas the blue arrows indicate the location of CdSe QDs.

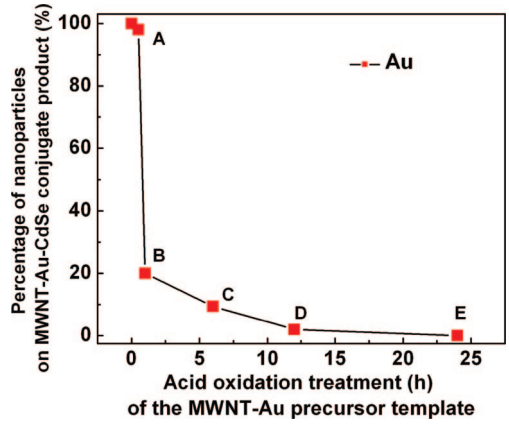

Figure 7. Relative percentage of Au nanoparticles vs CdSe nanocrystals on CNT surfaces in MWNT−Au−CdSe conjugates as a function of the oxidation time of the initial MWNT−Au precursor template in the presence of 1 M HNO_3. Data points (A−E) correspond to the TEM images shown in Figure 6.

an overall increase in percentage of CdSe QDs along the nanotube sidewalls in the final MWNT−Au−CdSe product.

Table 5. A Comparison of the Spatial Distribution and Coverage between Au Nanoparticles and CdSe Nanocrystals in MWNT−Au−CdSe Conjugates Upon Varying the Oxidation Times of the Initial MWNT−Au Precursor Templates

	oxidation time (h) of the MWNT−Au precursor template	percentage of nanoparticles along the sidewall	percentage of nanoparticles at the tips and ends	coverage of nanoparticles on MWNT surfaces (μm^{-1})
Au nanoparticles	0	94.6	5.4	20.3 ± 8.5
	0.5	93.3	6.7	18.0 ± 5.0
	1	94.5	5.5	12.0 ± 3.2
	6	95.0	5.0	5.0 ± 1.5
	12	100	0	2.3 ± 1.0
	24			0
CdSe nanocrystals	0			0
	0.5	100	0	0.5 ± 0.3
	1	91.0	9.0	48.0 ± 13.6
	6	94.9	5.1	48.2 ± 15.4
	12	94.2	5.8	50.0 ± 15.1
	24	94.1	5.9	50.9 ± 15.0

It should be mentioned that there was insufficient evidence to support a faster dissociation rate of Au nanoparticles at the tips as compared with the sidewalls. Nonetheless, given the same intrinsic probability of losing Au nanoparticles at both the tips and the sidewalls, the numerically lower quantity of particles localized at the tips, as compared with the sidewalls, would have led to an ostensibly more rapid replacement rate at the tip ends with CdSe quantum dots, which explains our data.

5.3. Hierarchical Synthesis of MWNT−CdSe−Au Conjugates. The converse reaction was also carried out. Specifically, H_2SO_4/HNO_3-treated MWNTs were first coated with CdSe QDs, followed by an additional oxidation process in 1 M HNO_3, and finally, incubation with Au NPs, so as to prepare MWNT−CdSe−Au conjugates illustrated in Figure 8A−E. That is, these conjugates were derived from MWNT−CdSe precursor templates that had been oxidized with nitric acid for 0.5, 1, 6, 12, and 24 h, respectively, prior to reaction and incubation with Au nanoparticles. As seen in Table 6, even though the loss of CdSe from the initial MWNT−CdSe was large, i.e., from 71.3 particles/μm to 9.8 particles/μm, the associated coverage of added Au did not increase in a proportionate manner, leveling off at around 13 particles/μm, consistent with a previous inference that the intrinsic size difference between Au and CdSe nanocrystals affected their overall density of coverage on the nanotube surface of the final product. Therefore, not surprisingly, we noted the percentage of CdSe QDs relative to that of Au NPs on the CNT surface decreased to a value of no less than 40%, even after a prolonged oxidation treatment of up to 24 h (Figure 9) of the initial MWNT−CdSe precursor template.

With respect to the spatial distribution of nanocrystals on the surfaces of the MWNTs, an initially high percentage of either CdSe QDs along the sidewalls of MWNTs (Table 6) was attributed to the formative H_2SO_4/HNO_3 treatment, that had resulted in a high level of defect sites. Subsequently, 6 h of 1 M HNO_3 treatment of the initial MWNT−CdSe conjugate resulted in a larger fraction of added Au nanoparticles localized at these tip regions (up to levels as high as 10.3%). At longer reaction times, i.e., oxidation times of the MWNT−CdSe precursor templates of up to 12 hours, we noted in the final product that defect sites, localized at

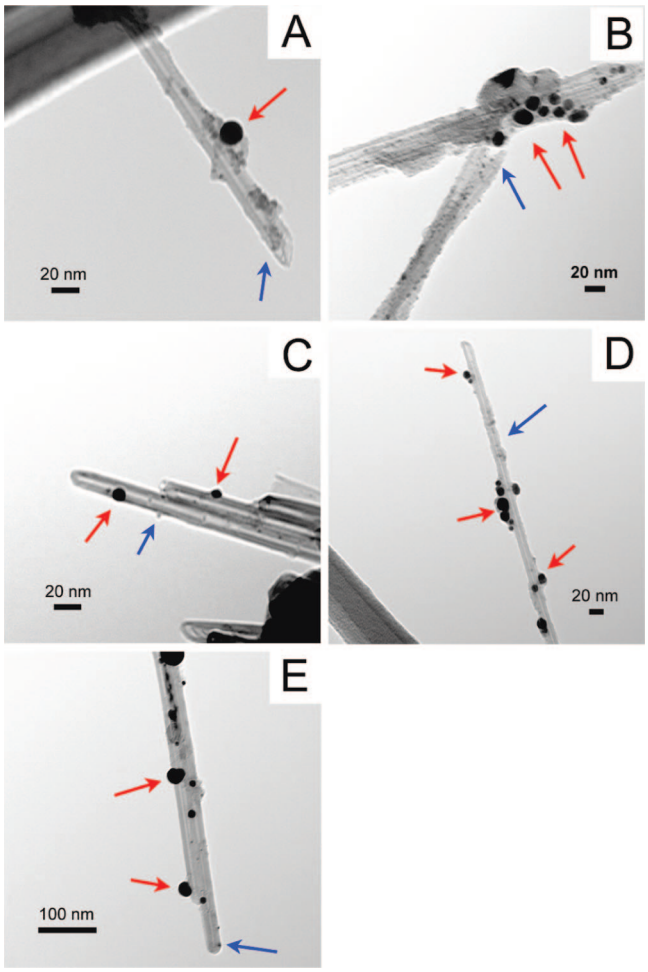

Figure 8. TEM images of MWNT−CdSe−Au conjugates. MWNT−CdSe conjugates were initially subjected to acid oxidation and subsequently thiolated prior to incubation with Au NPs for 2 h. Results are shown for MWNT−CdSe−Au products generated from MWNT−CdSe precursor templates, previously oxidized in 1 M HNO_3 for (A) 0.5 h, (B) 1 h, (C) 6 h, (D) 12 h, and (E) 24 h. The red arrows denote the presence of Au NPs whereas the blue arrows indicate the location of CdSe QDs.

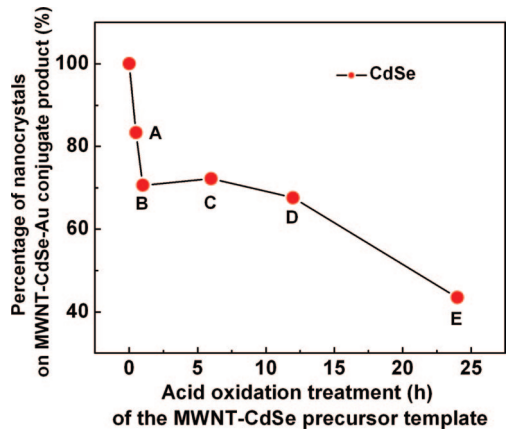

Figure 9. Relative percentage of CdSe nanocrystals vs Au nanoparticles on CNT surfaces in MWNT−CdSe−Au conjugates as a function of the oxidation time of the initial MWNT−CdSe precursor template in the presence of 1 M HNO_3. Data points (A−E) correspond to the TEM images shown in Figure 8.

the sidewalls, also began to fill up with added Au nanoparticles as CdSe QDs in these areas were being continuously removed by acid. We noted an 'equilibrium state', after 12 hours of initial oxidation of the MWNT−CdSe conjugate,

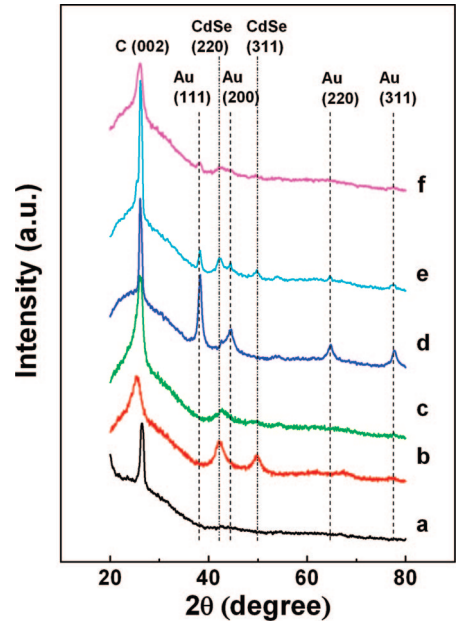

Figure 10. XRD patterns of (a) oxidized MWNTs, (b) AET−CdSe nanocrystals, (c) MWNT−CdSe conjugates, (d) MWNT−Au conjugates, (e) MWNT−Au−CdSe conjugates, and (f) MWNT−CdSe−Au conjugates. MWNTs were oxidized by H_2SO_4/HNO_3. For MWNT−Au−CdSe conjugates, MWNTs were first coated with Au NPs, oxidized in 1 M HNO_3 for 1 h, and finally coated with CdSe QDs. For MWNT−CdSe−conjugates, MWNTs were first coated with AET−CdSe, oxidized in 1 M HNO_3 for 1 h, and finally coated with Au NPs.

beyond which both the observed particle coverage as well as the spatial localization of either QDs or Au NPs remained relatively stable in the ultimate MWNT−CdSe−Au hierarchical assembly.

5.4. X-ray Diffraction. Figure 10 shows the XRD patterns of oxidized MWNTs, AET−CdSe nanocrystals, MWNT−CdSe conjugates, MWNT−Au conjugates, MWNT−Au−CdSe conjugates, and MWNT−CdSe−Au conjugates, in which the starting MWNTs were initially oxidized with H_2SO_4/HNO_3. As shown in Figure 10a, oxidized MWNTs possessed no obvious diffraction feature in the 2θ range between 30 and 80°. To clearly identify the CdSe peaks, the XRD pattern of AET−CdSe was displayed in Figure 10b, which was consistent with literature values of the bulk (JCPDS File 19−0191). Bragg diffraction peaks were all relatively broad because of the extremely small dimensions of the CdSe nanocrystals. For the MWNT−CdSe conjugates, in Figure 10c, peaks corresponding to the (220) and (311) reflections of CdSe indicated that CdSe nanocrystals were anchored onto CNT surfaces. For the MWNT−Au conjugates, peaks ascribable to (111), (200), (220), and (311) reflections of gold can be traced out in Figure 10d. Diffraction peaks for both Au NPs and CdSe QDs, though weak, are simultaneously present and highlighted in patterns e and f in Figure 10, suggestive of the successful formation of both MWNT−Au−CdSe and MWNT−CdSe−Au conjugates, respectively.

5.5. Optical Properties of Conjugates. Figure 11a−e indicates absorption spectra of oxidized MWNTs, MWNT−Au conjugates, MWNT−CdSe conjugates, MWNT−Au−CdSe conjugates, as well as CdSe QDs by means of comparison. The absorption spectrum of CdSe QDs showed a prominent excitonic transition at 610 nm, corresponding to a bandgap

Table 6. A Comparison of the Spatial Distribution and Coverage between Au Nanoparticles and CdSe Nanocrystals in MWNT−CdSe−Au Conjugates Upon Varying the Oxidation Times of the Initial MWNT−CdSe Precursor Templates

	oxidation time (h) of the MWNT−CdSe template	percentage of nanoparticles along the sidewall	percentage of nanoparticles at the tips and ends	coverage of nanoparticles on MWNT surface (μm^{-1})
Au nanoparticles	0			0
	0.5	100	0	8.0 ± 2.1
	1	91.7	8.3	8.7 ± 2.0
	6	89.7	10.3	13.4 ± 4.3
	12	96.3	3.7	12.0 ± 3.9
	24	95.2	4.8	13.0 ± 6.0
CdSe nanoparticles	0	96.6	3.4	71.3 ± 14.2
	0.5	97.8	3.2	50.0 ± 15.9
	1	89.5	10.5	32.2 ± 15.0
	6	96.9	3.1	29.0 ± 10.9
	12	97.5	2.5	25.0 ± 12.7
	24	96.8	3.2	9.8 ± 10.1

of 2.04 eV. The corresponding spectrum for oxidized MWNTs was broad and featureless. Relatively weak absorption peaks of MWNT−Au conjugates and MWNT−CdSe conjugates were noted at 520 nm and 600 nm, respectively, and magnified in the inset of Figure 11b and c. The absorption of CdSe in MWNT−CdSe conjugates was slightly blue-shifted, an observation that has been previously observed in MWNT systems coated with ZnO,[50] ZnS,[51] and CdS.[52]

In every case, this blue shift has been attributed to size quantization effects. The lower intensity of absorption may likely be due to an intrinsically lower concentration of nanocrystals on the MWNT surface as compared with what would be expected from a pure nanocrystal solution. The broad peak (Figure 11d) of MWNT−Au−CdSe centered at 576 nm was attributed to collective absorption due to both Au nanoparticles and CdSe QDs. The UV−visible data for all of our MWNT-based conjugates do not show any extraneous features that would typically arise from either charge diffusion or electronic interaction between nanotubes and quantum dots in their ground states.[53]

To further investigate the optical properties of our as-prepared conjugates, the photoluminescence behavior (PL) of the MWNT and AET−CdSe constituent components as well as the resulting MWNT−CdSe and MWNT−Au−CdSe conjugates was measured upon illumination at 400 nm, as shown in Figure 12a−d. One motivation for our work is that MWNTs attached directly to Cu_2S nanocrystals were thought to facilitate the generation of a photocurrent by trapping conduction band electrons, a process known to enhance charge separation and retardation of the recombination process.[54] A substantial decrease in the PL intensity was observed for both MWNT−CdSe and MWNT−Au−CdSe conjugates (spectra b and c in Figure 12) as compared with the AET−CdSe starting material (Figure 12d), which possessed an intense band-edge emission peak at 612 nm.

In fact, the emission of the CdSe appears to be totally quenched when these CdSe QDs were bound covalently to the MWNTs, suggesting a strong excited-state interaction with the nanotubes. The featureless fluorescence signal for MWNT−CdSe conjugates is in agreement with prior literature on SWNTs.[6,25,55] That is, to explain the observed emission quenching, the deactivation process of photoexcited CdSe nanoparticles can be attributed to an appreciable and rapid electron transfer and charge injection from the excited semiconductors into the MWNT platform.[8,56] Specifically, photoinduced electrons upon illumination of CdSe formed electron−hole pairs which could then undergo a normal radiative recombination process. However, once MWNTs were brought into contact with these excited QDs, the nonradiative quenching process, due to electron flow from the conduction band of electron donating QDs to empty

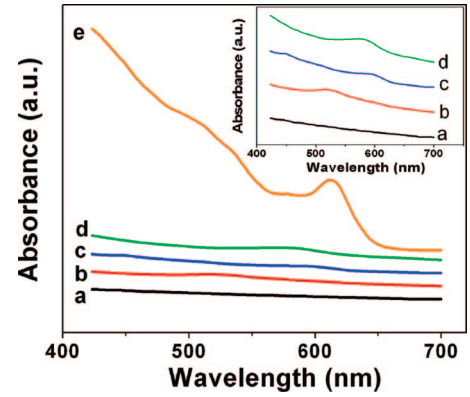

Figure 11. UV−visible spectra of (a) oxidized MWNTs (black curve), (b) MWNT−Au conjugates (red curve), (c) MWNT−CdSe conjugates (blue curve), (d) MWNT−Au−CdSe conjugates (green curve), and (e) CdSe QDs (orange curve). MWNTs were initially oxidized by H_2SO_4/HNO_3. Inset: Magnified absorption spectra corresponding to nanotube-based systems (a−d).

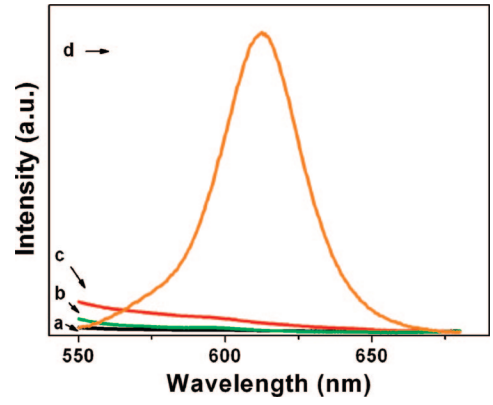

Figure 12. Photoluminescence spectra of (a) raw MWNTs (black curve), (b) MWNT−Au−CdSe conjugates (green curve), (c) MWNT−CdSe conjugates (red curve), and (d) AET−CdSe nanocrystals (orange curve). MWNTs were initially oxidized by H_2SO_4/HNO_3. Excitation wavelength used is 400 nm. The spectra were normalized at a wavelength of 680 nm.

(50) Jiang, L. Q.; Gao, L. *Mater. Chem. Phys.* **2005**, *91* (2−3), 313–316.
(51) Shan, Y.; Gao, L. *J. Am. Ceram. Soc.* **2006**, *89* (2), 759–762.
(52) Liu, B.; Lee, J. Y. *J. Phys. Chem. B* **2005**, *109* (50), 23783–23786.
(53) Olek, M.; Busgen, T.; Hilgendorff, M.; Giersig, M. *J. Phys. Chem. B* **2006**, *110* (26), 12901–12904.

electronic states of the electron accepting nanotubes, became competitive with the intrinsic radiative decay process, thereby resulting in the observed decrease in the PL intensity of the CdSe.[53] The overall point is that efficient charge separation and transport can be achieved in these nanoscale conjugate systems.

In addition, it has been proposed that nanotubes can also act as energy sinks for attached nanoparticles/nanocrystals through an excited-state energy transfer mechniasm due to the effect of the nanotubes' electron accepting ability.[57] It is noted, however, that the extent of energy transfer depends on the interparticle distance (r^{-6} dependence) between QDs and CNTs and represents an alternative pathway for quenching of the CdSe emission.[58] In our case, the PL of CdSe QDs could also have been quenched by our use of relatively short linkers (e.g., AET) bridging the CdSe and oxidized MWNTs.

To rule out the possibility that either the presence or introduction of free ligands from the QDs might have partially offset the emission quenching and returned the CdSe PL signal to a measurable level, the PL spectrum of MWNT−CdSe conjugates was taken in the presence of free AET molecules at a concentration of 0.5 M. No peak was observed. Moreover, we should note that any extraneous, unbound CdSe QDs as well as corresponding free ligands were likely removed from the system, prior to our optical experiments by extensive washing steps. As such, therefore, the presence of either free CdSe QDs or free ligands likely did not interfere with the observed optical data associated with our nanotube−nanocrystal conjugates.

Overall, our MWNT−Au−CdSe conjugate is analogous to a previously reported CdS−Au−TiO_2 three-component nanojunction system which exhibits high photocatalytic activity due to vectorial electron transfer driven by a two-step excitation of TiO_2 and CdS.[59] Of particular relevance to our nanotube-based conjugate (Figure 12), it has been demonstrated that photoluminescence quenching of CdSe QDs by Au nanoparticles themselves can occur via either energy-transfer[60] or electron-transfer[61] mechanisms.

For our MWNT−Au−CdSe conjugates, we noted that in some of our composites, CdSe QDs were in close physical proximity to adjoining Au NPs because of the spatial distribution of defect sites on the surfaces of the MWNTs. Thus, it is not surprising to find that the fluorescence of CdSe was greatly suppressed for MWNT−Au−CdSe conjugates, as the emission of CdSe QDs was likely quenched by the presence of both MWNTs and Au NPs.

6. Conclusions

We have demonstrated a covalent route toward site-selective synthesis of MWNT−nanoparticle conjugates containing two different types of nanoscale species, i.e., Au nanoparticles and CdSe QDs. We have quantitatively probed the effects of varying oxidation treatments, precursor concentrations, and incubation times in order to rationally affect the spatial coverage and distribution of either Au NPs or semiconducting QDs on the MWNT sidewalls and tips. The degree of nanoparticulate coverage was found to primarily vary with the intensity of the oxidation treatment, though the hydrophobicity of the nanotube as well as the chemical and steric characteristics of the nanocrystals also played a role in determining the ultimate architecture. In general, the stronger the oxidation treatment, the denser the coating of nanoparticles and/or quantum dots on the nanotube surface. In addition, the use of larger concentrations of precursor nanocrystals along with longer incubation times was also conducive to the observation of higher nanoparticle densities on our nanotube templates. Furthermore, our overall results suggested that it was the precise nature of the oxidation treatment that primarily affected the spatial distribution of nanoparticles either at the ends or along the sidewalls of the carbon nanotubes.

Although none of these trends were perfect, our findings suggest a reasonable way of fabricating a series of novel CNT−nanocrystal/nanoparticle heterostructure composites with potentially tailorable electronic or optical properties. Moreover, by controllably varying the oxidation time of MWNT−Au/CdSe precursor templates, MWNT−Au−CdSe and MWNT−CdSe−Au conjugates with different percentages of NPs and QDs, purposely localized either along the ends or sidewalls, could be obtained. Interesting charge-transfer as well as energy-transfer behaviors between CNTs and the corresponding nanoparticles/quantum dots have been observed[62,63] and will likely render such conjugates as key components in a range of nanoscale devices important for photocatalytic and solar applications.

Acknowledgment. We acknowledge the U.S. Department of Energy (DE-AC02-98CH10886) for facility and personnel support. We also thank the National Science Foundation (CAREER Award DMR-0348239), and the Alfred P. Sloan Foundation for PI support and experimental supplies. Moreover, we are grateful to D. Wang (Boston College) as well as to F. Zhang and S. van Horn (SUNY Stony Brook) for their assistance with electron microscopy.

Supporting Information Available: Additional experimental details and Figures S1−S7 (PDF). This material is available free of charge via the Internet at http://pubs.acs.org.

CM802648M

(54) Lee, H.; Yoon, S. W.; Kim, E. J.; Park, J. *Nano Lett.* **2007**, *7* (3), 778–784.
(55) Robel, I.; Bunker, B. A.; Kamat, P. V. *Adv. Mater.* **2005**, *17* (20), 2458–2463.
(56) Vietmeyer, F.; Seger, B.; Kamat, P. V. *Adv. Mater.* **2007**, *19*, 2935–2940.
(57) Gu, F.; Li, C. Z.; Wang, S. F. *Inorg. Chem.* **2007**, *46* (13), 5343–5348.
(58) Pan, B. F.; Cui, D. X.; Ozkan, C. S.; Ozkan, M.; Xu, P.; Huang, T.; Liu, F. T.; Chen, H.; Li, Q.; He, R.; Gao, F. *J. Phys. Chem. C* **2008**, *112* (4), 939–944.
(59) Tada, H.; Mitsui, T.; Kiyonaga, T.; Akita, T.; Tanaka, K. *Nat. Mater.* **2006**, *5* (10), 782–786.
(60) Kondon, M.; Kim, J.; Udawatte, N.; Lee, D. *J. Phys. Chem. C* **2008**, *112* (17), 6695–6699.
(61) Costi, R.; Saunders, A. E.; Elmalem, E.; Salant, A.; Banin, U. *Nano Lett.* **2008**, *8*, 637–641.
(62) Lee, J.; Javed, T.; Skeini, T.; Govorov, A. O.; Bryant, G. W.; Kotov, N. A. *Angew. Chem., Int. Ed.* **2006**, *45* (29), 4819–4823.
(63) Govorov, A. O.; Bryant, G. W.; Zhang, W.; Skeini, T.; Lee, J.; Kotov, N. A.; Slocik, J. M.; Naik, R. R. *Nano Lett.* **2006**, *6* (5), 984–994.